An experimental study of flow and heat transfer in a differentially side heated cavity filled with coarse porous media

Ataei-Dadavi, Iman; Rounaghi, Nima; Chakkingal, Manu; Kenjeres, Sasa; Kleijn, Chris R.; Tummers, Mark J.

DOI
10.1016/j.ijheatmasstransfer.2019.118591

Publication date
2019

Document Version
Final published version

Published in
International Journal of Heat and Mass Transfer

International Journal of Heat and Mass Transfer 143 (2019) 118591

Contents lists available at ScienceDirect

International Journal of Heat and Mass Transfer

journal homepage: www.elsevier.com/locate/ijhmt

An experimental study of flow and heat transfer in a differentially side heated cavity filled with coarse porous media

Iman Ataei-Dadavi [a,*], Nima Rounaghi [a], Manu Chakkingal [a], Sasa Kenjeres [a], Chris R. Kleijn [a], Mark J. Tummers [b]

[a] Department of Chemical Engineering, Delft University of Technology, Van der Maasweg 9, 2629HZ Delft, the Netherlands
[b] Department of Process and Energy, Delft University of Technology, Leeghwaterstraat 39, 2628CB Delft, the Netherlands

ARTICLE INFO

Article history:
Received 12 March 2019
Received in revised form 14 August 2019
Accepted 15 August 2019

Keywords:
Natural convection
Heat transfer
Differentially heated cavity
Porous media
Packed beds
Refractive index matching

ABSTRACT

Flow and heat transfer in a differentially side heated cubic cavity filled with relatively large solid spheres forming a coarse porous medium have been studied experimentally. Nusselt numbers were measured for Rayleigh numbers between 1.9×10^7 and 1.7×10^9, solid-to-fluid conductivity ratios between 0.32 and 618, and for different sphere sizes ($d/H = 0.065$, 0.14, 0.20), and packing geometries. The heat transfer results indicate that the presence of a porous medium in the cavity decreases the heat transfer compared to the pure-fluid cavity unless the solid spheres are highly conductive. We present a new Nusselt number correlation for coarse porous media based on porous medium dimensionless numbers. Particle image velocimetry and liquid crystal thermography measurements were performed in a refractive index-matched porous medium to obtain pore-scale velocity and temperature fields. The results show that the layers of spheres adjacent to the hot/cold walls play the most prominent role in the heat transfer reduction by hindering the formation of high-velocity boundary layers along the hot/cold walls, causing a portion of the boundary layer fluid to divert away from these walls, thus changing the stratified temperature distribution to a tilted one which leads to a lower overall heat transfer.

1. Introduction

Natural convection in enclosures differentially heated from the sides and containing porous media or solid obstacles has attracted a great deal of attention due to its fundamental nature and the broad range of applications in, for example, iron and steel making [1], food processing [2], electronics cooling [3], and indoor air conditioning [4].

Most theoretical and computational studies in the field of natural convection in differentially side heated cavities filled with porous media have been based on Darcy's law and its extensions to include inertia and viscous diffusion effects (Forchheimer and Brinkman modifications), using so-called volume averaging over representative elementary volumes (REVs) [5–8]. This is a suitable approach when the pore length scale is much smaller than the macroscopic flow length scales. Lauriat and Prasad [6] numerically solved the Darcy-Brinkman-Forchheimer equations for a differentially heated cavity and reported that the heat transfer rate always increases with the fluid Rayleigh number, Ra, the Darcy number, Da, and the effective thermal conductivity of the porous medium, k_{eff}. They concluded that a porous medium can transport more heat than a pure fluid if the porous matrix is highly permeable and the thermal conductivity of solid particles is higher than that of the fluid.

There are only a few experimental studies on natural convection in differentially side heated cavities filled with porous media and these are limited to heat transfer measurements to verify the mentioned theoretical and computational models [9,10].

Other researchers have studied natural convection in 2D differentially side heated enclosures containing disconnected solid objects [3,11–14]. They considered solid and fluid constituents separately and solved the Navier-Stokes equations to obtain detailed information on the interaction between the flow and temperature fields with the discrete solid objects. Merrikh and Lage [11] numerically studied natural convection in a differentially heated square enclosure containing several disconnected and conducting solid blocks for Rayleigh numbers between 10^5 and 10^8 and solid-to-fluid conductivity ratios between 0.1 and 100. They found that the flow tends to migrate away from the vertical hot/cold walls and penetrates into the interior channels as the number of blocks increases (and the size of the blocks decreases). They derived an analytical expression for the minimum number of blocks necessary for the flow to divert from the hot/cold walls.

* Corresponding author.
E-mail address: i.ataeidadavi@tudelft.nl (I. Ataei-Dadavi).

https://doi.org/10.1016/j.ijheatmasstransfer.2019.118591
0017-9310/

Raji et al. [14] carried out a similar numerical study for Rayleigh numbers $10^3 \leq Ra \leq 10^8$, solid-to-fluid conductivity ratios $10^{-3} \leq k_s/k_f \leq 10^3$, and a varying number of solid blocks. They observed that by increasing the number of blocks the heat transfer and flow intensity are significantly reduced, especially at low and moderate Rayleigh numbers ($Ra \leq 10^5$). They also reported that the blocks with lower conductivity enhance the convection heat transfer.

With the above literature focusing on either Darcy-type modeling of convection and heat transfer in fine-grained porous media with an REV approach, or on convection around disconnected coarse-grained solid objects, in many applications natural convection occurs in porous media consisting of relatively large solid objects which are in contact with each other. Examples include stacks of agricultural products for drying or in cold storages [15] and relatively large coke particles in the hearth of blast furnaces [16]. In the chain of steel production, the blast furnace converts iron ore into hot liquid iron. The furnace hearth has a coarse-grained porous carbon structure with a typical grain size up to 100 mm. With the hot metal flowing in from the top and the walls of the hearth being cooled, the flow of liquid metal in the hearth is a natural convection flow in a coarse-grained porous medium. This flow can cause erosion of refractory walls due to the local wall heat transfer non-uniformities (hot spots). This has a severe impact on the lifetime of the blast furnaces. For such coarse-grained porous media, the REV approach and the use of (extended) Darcy laws are questionable. Therefore, Laguerre et al. [17] compared direct CFD and volume averaged Darcy-Brinkman-Forchheimer to experiments for natural convection in a differentially side heated enclosure filled with a $6 \times 6 \times 5$ cubic arrangement of spheres at $Ra = 2.3 \times 10^8$. Both modeling approaches were found to lead to good agreement with fluid and solid temperatures measured at various locations using thermocouples. Velocities in the pores between the spheres, however, could not be measured to validate the CFD velocity results.

Indeed, visualizing natural convection flow in porous media has always been a challenge. Shattuck et al. [18] measured vertically-averaged vertical velocities in bottom-heated natural convection cells filled with packings of spheres using magnetic resonance imaging (MRI). Laguerre et al. [19] used Particle Image Velocimetry to partially visualize the air flow in a differentially heated rectangular cavity containing cylindrical obstacles which occupied about 15% of the cavity volume. They were not able to visualize the areas behind the obstacles and also at the bottom of the cavity since the laser light sheet was blocked by the obstacles and a support plate at the bottom. Recently, experimental [20] and numerical [21] studies have investigated detailed flow and temperature structures in bottom-heated natural convection cavities filled with relatively large spheres.

In summary, there are still many open questions regarding differentially side-heated natural convection flow and heat transfer in media with a relatively large porous length scale, where (extended) Darcy models are not valid and the relatively large solid particles are in contact with each other. For such systems, the heat transfer, the pore-scale flow structure and the interaction between natural convection flow and coarse-grained porous media need to be studied in more detail. Detailed experimental data on flow and heat transfer are also required for the development and validation of computational models.

The objective of the present study is to improve the understanding of differentially side heated natural convection flow and heat transfer in coarse porous media in the form of a packed bed of relatively large spheres. We carried out a series of heat transfer measurements in a differentially side heated cubic $H \times H \times H$ cavity to identify the effect of different parameters such as sphere size ($d/H = 0.065–0.20$), solid-to-fluid conductivity ratio ($k_s/k_f = 0.32–618$), and packing structure on the overall heat transfer. To obtain detailed information on the pore-scale velocity and temperature distribution throughout the porous medium we performed Particle Image Velocimetry (PIV) and Liquid Crystal Thermography (LCT) measurements in a refractive index matched porous medium (hydrogel spheres in water).

2. Experimental setup

The experimental setup is very similar to our recent work and is described in [20] in more details. Herein, only the main and novel features of the experimental setup will be described. The same cubical cavity with internal dimensions of $77 \times 77 \times 77$ mm^3 was used in all the experiments (see Fig. 1a). The main difference is that in the present study the cavity is rotated over 90° resulting in a differentially side heated configuration. The left and right walls of the cavity are made of copper plates, serving as isothermal hot wall and cold wall, respectively. The other four walls are made of glass. The left wall was heated with an electrical heating foil attached to the copper plate. Cold water from a thermostatic bath flows through channels inside the right wall to keep it at a lower temperature. The temperatures of the isothermal walls were measured with Pt100 temperature sensors with an inaccuracy of ± 0.03 °C. The temperature non-uniformities were measured to be below 0.06 °C for the hot wall and below 0.02 °C for the cold wall.

In the heat transfer measurements, the temperature difference ΔT between the isothermal walls, and the electrical power of the heating foil, P, were used to obtain the Rayleigh and Nusselt numbers. The overall Nusselt number Nu is determined by subtracting the total heat loss Q_{loss} from the electrical power supplied to the heating foil as in

$$Nu = (P - Q_{loss})/(A_f k_f \Delta T/H), \quad (1)$$

where H is the height of the cubical cavity (77 mm), and k_f is the thermal conductivity of the fluid. A_f is the internal cross-sectional area of the cavity $A_f = H^2$. The electrical power of the heating foil, P, was determined by measuring the electrical current and the voltage difference at the electrical connections near the heating foil. The total heat loss Q_{loss} was determined by performing experiments in the same cavity with the hot plate at the top and the cold plate at the bottom filled with the working fluids (water or methanol). In this configuration, the convective heat transfer is zero and only conduction takes place. The heat that is supplied in addition to the expected fluid conductive heat transfer was taken as the total heat loss.

Using the temperature difference between the hot and cold walls, ΔT, the Rayleigh number Ra is determined as

$$Ra = \beta \Delta T g H^3/(\alpha \nu), \quad (2)$$

where β is the thermal expansion coefficient of the fluid, g is the gravitational acceleration, ν is the kinematic viscosity of the fluid and α is its thermal diffusivity. The Nusselt number and the Rayleigh number in Eqs. (1) and (2) are defined based on the fluid properties rather than the porous medium properties. In this way, the overall heat transfer results can be compared to that of the pure-fluid cavity. In the experiments, the Rayleigh number was varied in the range $1.9 \times 10^7 \leq Ra \leq 1.7 \times 10^9$. The first decade was achieved by varying ΔT using water as a working fluid, and the second decade was reached by varying ΔT using methanol. The two fluids have very similar Prandtl numbers, i.e. $Pr_{water} = 6.75$; $Pr_{methanol} = 7.63$ at 22 °C. The maximum uncertainties in the measured values of the Rayleigh and Nusselt numbers occur at the lowest temperature difference and are equal to 2.8% and 3.0%, respectively.

Four different sphere solid materials (polypropylene, glass, steel, and brass), three different sphere sizes (5.0 mm, 10.5 mm,

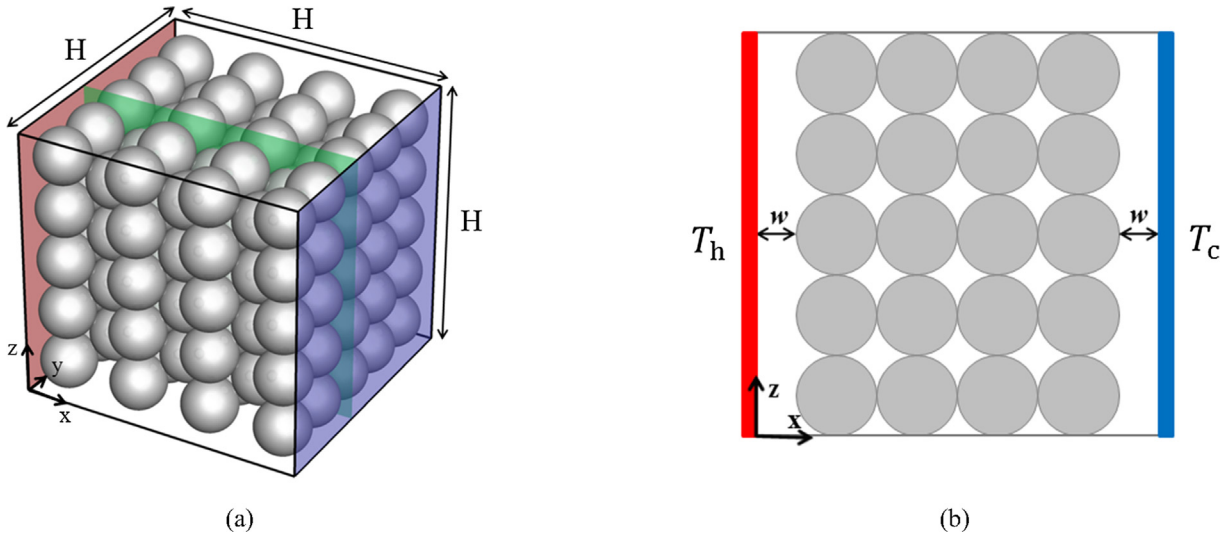

Fig. 1. (a) Sketch of the test cavity filled with spheres with size $d/H = 0.20$ in body-centered tetragonal (BCT) packing, and the location of the light sheet in the PIV/LCT measurements at $y/H = 0.4$. (b) Front view of the 3D printed $4 \times 5 \times 5$ simple cubing packing with a gap of $w/H = 0.10$ between the porous medium and the hot/cold walls.

and 15.3 mm, corresponding to $d/H = 0.065$, 0.14, and 0.20), and three different packing structures were examined in the heat transfer measurements. The spheres were packed in simple cubic (SC), body-centered tetragonal (BCT) (see Fig. 1a), and random packing structures. To study the effect of a gap between the hot/cold walls and the porous medium, a $4 \times 5 \times 5$ simple cubic packing structure of 15.3 mm polypropylene spheres was build using a 3D printer (Seido Systems Object500 Connex 3), see Fig. 1b.

In Section 3.1.5, a heat transfer scaling based on porous medium dimensionless groups is presented. These porous medium dimensionless numbers are defined as

$$\mathrm{Ra_m} = \mathrm{Ra\ Da\ k_f/k_{eff}}, \tag{3}$$

and

$$\mathrm{Nu_m} = \mathrm{Nu\ \ k_f/k_{eff}}, \tag{4}$$

where Da is the Darcy number defined as $\mathrm{Da} = K/H^2$ and K is the permeability of the packed bed of spheres. The value of K is estimated using the Ergun expression [22], $K = \phi^3 d^2/(150(1-\phi)^2)$, where ϕ is the porosity of the packed bed and d is the diameter of the spheres. In Eqs. (3) and (4), k_{eff} is the effective thermal conductivity of the porous medium which is defined as the overall thermal conductivity through the combination of solid and fluid constituents, in the absence of fluid motion. As discussed in [20], the effective thermal conductivities for the geometries and the solid-fluid combinations considered in this study were numerically computed from the 3D heat conduction equation for solid and stagnant fluid. For completeness, the resulting values are shown again in the present paper in Table 1.

Table 1
Ratio of Solid to fluid conductivity k_s/k_f and ratio of porous medium to fluid conductivity k_{eff}/k_f for the different combinations of solids and fluids considered in this study.

Sphere and fluid materials	$\frac{k_s}{k_f}$	$\frac{k_{eff}}{k_f}$
Brass - Methanol	618	17.3
Steel - Methanol	222	14.0
Brass - Water	196	13.6
Steel - Water	70.4	9.45
Glass - Methanol	4.19	2.30
Glass - Water	1.33	1.22
Polypropylene - Methanol	1.00	1.00
Polypropylene - Water	0.32	0.79

To be able to visualize the flow in between the spheres at the core of the porous media, we used water as the liquid and hydrogel spheres - which consist of approximately 99.5% water, are transparent and have virtually the same refractive index as that of water – for the solid packing. This makes the porous medium optically accessible both for illumination and imaging, thus enabling the use of the optical measurement techniques PIV and LCT. As discussed in our recent work [20], the advantage of using water as working fluid, over frequently-used refractive index matching liquids, is that the refractive index of water has the lowest sensitivity to temperature variations which makes it an ideal liquid for refractive index matching to study a thermally-driven flow. As a result, the refractive index of the hydrogel spheres matches the refractive index of water at various temperatures with a difference less than 0.1%.

In the PIV and LCT experiments, hydrogel spheres with a diameter of approximately 15.3 mm ($d/H = 0.20$) were arranged in a BCT packing. The measurements were performed in a vertical plane at $y/H = 0.4$ (see Fig. 1a).

The same PIV system as described in [20] was used to obtain velocity fields with high spatial resolution. Velocity vectors were calculated from the raw images based on a multi-pass cross-correlation with a final interrogation window size of 16×16 pixels and an overlap of 50% using the LaVision software (Davis 8.4.0). The resulting vector spacing resolution is 0.60 mm.

LCT measurements were performed to obtain planar temperature fields inside the cavity. The LCT experimental setup is described in details in [20]. In the lightsheet configuration with a 90° viewing angle, the measurable temperature range of the liquid crystals was found to be between 20.0 °C and 30.2 °C. Fully making use of this temperature range leads to $\Delta T = 10.2$ °C and hence $\mathrm{Ra} = 9.0 \times 10^7$.

Temperature-hue calibration as described in [20] was carried out to quantitatively determine temperatures from the LCT color images. The uncertainty of the measured temperatures was estimated to be ±0.5 °C.

3. Results and discussion

3.1. Heat transfer measurements

Fig. 2 presents the Nu-Ra data points obtained from heat transfer measurements in the side-heated cavity filled with

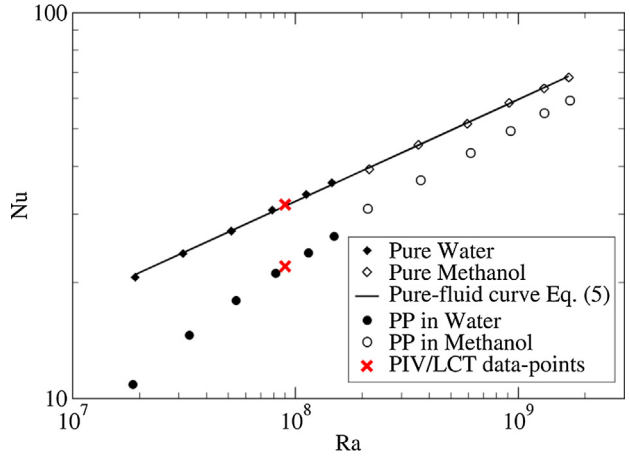

Fig. 2. Nu-Ra data for the differentially side-heated cubic cavity filled with a porous medium consisting of 15.3 mm ($d/H = 0.20$) polypropylene (PP) spheres in BCT packing, compared to that for the pure-fluid cavity. The measurements in water and methanol are indicated by closed and open markers, respectively. The solid line denotes the fit to the Nu-Ra data for the pure-fluid cavity, Eq. (5). The red crosses pertain to the PIV and LCT measurements described in Section 3.2.

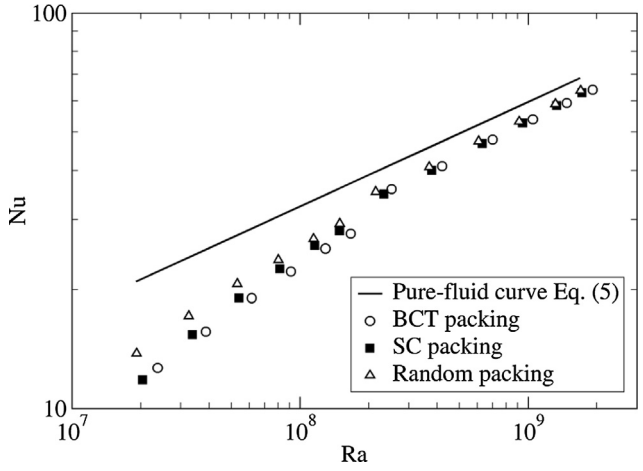

Fig. 3. Effect of packing. Nu-Ra data for porous media consisting of 15.3 mm ($d/H = 0.20$) glass spheres with three different packing types. The solid line denotes the fit to the Nu-Ra data for the pure-fluid cavity, Eq. (5).

15.3 mm ($d/H = 0.20$) polypropylene spheres in BCT packing, along with the results obtained from the same cavity filled with the fluids only. In this figure, the results obtained in water (lower Ra range) and in methanol (higher Ra range) are depicted by closed and open markers, respectively. In the remainder of the paper, we do not distinguish between measurements in water and methanol and use the same marker for both. The Nu-Ra data for the pure-fluid cavity are fitted well by a power-law

$$\mathrm{Nu} = 0.250\mathrm{Ra}^{0.264} \tag{5}$$

for $1.9 \times 10^7 < \mathrm{Ra} < 1.7 \times 10^9$. The maximum deviation of the experimental data from the power-law curve is 1.2%. This relation agrees well with the findings of studies on differentially side heated cubic cavities in this range of Rayleigh numbers [23,24]. The power-law curve, Eq. (5), is presented as a solid line in Fig. 2 and is used as a reference curve in the rest of the paper.

Fig. 2 clearly shows that the addition of polypropylene spheres to the cavity reduces the Nusselt number compared to that for the pure-fluid cavity. The reduction continues to exist at Rayleigh numbers as high as 1.7×10^9. This is in contrast to what has been found for the same porous medium in a bottom-heated cavity [20], where it was observed that Nusselt values for the same sphere size ($d/H = 0.20$) reach (and even slightly exceed) those of the pure-fluid bottom-heated cavity at $\mathrm{Ra} > 6 \times 10^8$. This implies that the interaction between the natural convection flow and porous media in the side-heated cavity is very different from that in the bottom-heated cavity.

3.1.1. Effect of packing type

To study the influence of the type of packing on Nusselt number in a side-heated cavity, three different packing types were examined: BCT packing, SC packing, and a random packing. Glass spheres with a diameter of 15.3 mm ($d/H = 0.20$) were used to make these packings. In the small cubical cavity considered in this study, a BCT packing resulted in a porosity of $\phi = 42.0\%$, a simple cubic packing in $\phi = 48.6\%$, and a random packing in $\phi = 49.8\%$. Fig. 3 shows the Nusselt number as a function of Rayleigh number for the three packings along with the pure-fluid reference curve, Eq. (5). It can be observed that the Nusselt numbers are slightly higher for random packing, which has the highest porosity and permeability, and it is lower for BCT packing, which is the least permeable packing. The results generally imply that Nusselt number in packed beds of spheres is not largely influenced by the type of packing. This is due to the fact that the arrangements of the spheres adjacent to the hot/cold walls are very similar in all the three different packing structures. In both BCT and SC packings, the spheres have the same 5×5 arrangement at the hot/cold walls, whereas in random packing - due to the large value of d/H and the effects of wall constraints - the spheres are spontaneously arranged in a similar way. While at the lowest Rayleigh number the largest difference in the Nusselt numbers of the three different packings is approximately 14%, the difference is less than 3% at the highest Rayleigh number. This behavior implies that as Rayleigh increases, the Nusselt number becomes more independent of the packing structure.

3.1.2. Effect of sphere size

To study the effect of the size of the spheres on the Nusselt number, glass spheres with three different sizes $d = 15.3$ mm, $d = 10.5$ mm, and $d = 5.0$ mm ($d/H = 0.20$, 0.14, and 0.065) in random packings have been examined. The resulting porosity values are $\phi = 49.8\%$, $\phi = 45.3\%$, and $\phi = 42.1\%$, respectively. The corresponding Nu-Ra data points are included in Fig. 4, which shows that the Nusselt number reduces with decreasing sphere size. The heat transfer reduction occurs over the entire range of Rayleigh number, but the reduction is strongest at lower Rayleigh numbers. This can be explained by the fact that, although the overall porosities for the three studied sphere sizes are not very different, the local porosities near the hot/cold vertical walls are much lower for the 5 mm ($d/H = 0.065$) spheres compared to those for 15.3 mm ($d/H = 0.20$) spheres.

3.1.3. Effect of a gap between the hot/cold walls and the porous medium

A 3D printed $4 \times 5 \times 5$ simple cubic packing of 15.3 mm ($d/H = 0.20$) plastic spheres was placed in the cavity to create a gap between the porous medium and the thermally active hot/cold vertical walls. The (dimensionless) gap size is $w/H = 0.10$, which is larger than the thickness of the thermal and velocity boundary layers obtained from $\delta_T/H = \mathrm{Ra}^{-1/4}$ and $\delta_v = \mathrm{Pr}^{1/2}\delta_T$ [25]. For the working fluids used in this study $\mathrm{Pr} > 1$ so that the velocity boundary layer will be thicker than the thermal boundary layer. The thickness of the velocity boundary is $\delta_v/H \sim 0.039$ at the lowest Rayleigh number, and $\delta_v/H \sim 0.014$ at the highest Rayleigh number. The Nu-Ra data points obtained from this configuration are plotted in Fig. 5, along with the pure-fluid reference curve and

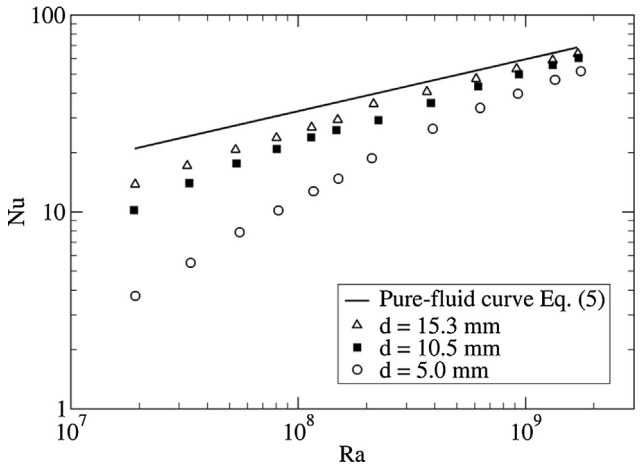

Fig. 4. Effect of sphere size. Nu-Ra data for porous media consisting of three different sizes of glass spheres in random packings compared to the pure-fluid reference curve.

the results from the porous medium consisting of 15.3 mm polypropylene spheres without the gap. The figure clearly shows that creating a sufficiently large gap near the thermally active walls can substantially enhance the Nusselt number with respect to the case where the spheres touch these walls. While in the packing without gap the Nusselt number is reduced by 53% at the lowest Ra, and by 13% at the highest Rayleigh number with respect to the pure-fluid cavity, the reduction is only 11% and 0.6% for the cases with a gap between the hot/cold walls and the porous medium. In other words, when the hot/cold walls are not covered by the porous medium, the heat transfer reduction is significantly smaller, and at the highest Rayleigh numbers ($Ra > 10^9$) the Nusselt values reach those for the pure-fluid cavity. The reduction of the Nusselt number at low Rayleigh numbers can be explained by the fact that heat should be convected horizontally from one side of the cell to the other side through the porous medium. At low Rayleigh numbers, the flow length scales are large compared to the pore length scale. Therefore, the flow cannot easily penetrate into the pores and, consequently, the convective transfer of heat in the horizontal direction through the porous medium is hampered. In general, it can be understood that the spheres located close to the vertical hot/cold walls play the most hindering role in the heat transfer mechanism. These observations imply that the interaction between the natural convection flow and the spheres near the hot/cold walls determines most of the heat transfer reduction in a side-heated cavity filled with spheres.

3.1.4. Effect of conductivity ratio

To study the effect of the solid-to-fluid conductivity ratio in a coarse-grained porous media filled side heated cavity, porous media consisting of 15.3 mm spheres made from four different materials were placed in water and methanol in a BCT packing. The four materials are polypropylene, glass, steel, and brass, with the solid-to-fluid conductivity ratios k_s/k_f listed in Table 1. Fig. 6 presents the Nu-Ra data points for the four materials along with the pure-fluid curve as a reference. Small discontinuities can be observed at the transition from water to methanol (around $Ra = 2 \times 10^8$), due to the associated jump in k_s/k_f. The results show that the Nusselt number increases with increasing conductivity ratio, for the entire range of Rayleigh numbers considered in this study. It is also observed that if a porous medium consists of highly conductive spheres, it can transport more heat compared to the pure-fluid cavity at sufficiently high Rayleigh numbers. The increased heat transfer is due to the contribution of both conductive and convective heat transfer. In the studied cases, the heat transfer enhancement at the highest Rayleigh number with respect to the pure-fluid cavity is 29% for the brass spheres and 20% for the steel spheres. For the case with $k_s/k_f = 1$, the heat transfer reduction with respect to the pure-fluid cavity is 14% at the highest Rayleigh number.

The Nusselt number dependency on the conductivity ratio k_s/k_f at a low ($Ra = 2.0 \times 10^7$), an intermediate ($Ra = 2.0 \times 10^8$), and a high ($Ra = 1.7 \times 10^9$) Rayleigh number is plotted in Fig. 7 by examining different combinations of the four solid materials and the two fluids. It is observed that the Nusselt number increases with solid-to-fluid conductivity ratio at all Rayleigh numbers. Fig. 7 shows that the equations that fit the data-points for all the three Rayleigh numbers are in the form of

$$Nu = Nu_0(1 + k_s/k_f)^m. \quad (6)$$

Nusselt number asymptotically approaches a constant value of Nu_0 as k_s/k_f goes to zero which represents the cavity filled with adiabatic spheres, where heat transfer is merely due to the fluid convection. The asymptotic values Nu_0 are found to be 10.6, 28.8, and 55.6 for the low, the intermediate, and the high Rayleigh numbers, respectively. Fig. 7 also shows that as the Rayleigh number increases, the Nusselt number dependency on solid-to-fluid conductivity ratio decreases. This is reflected in a decrease of the value

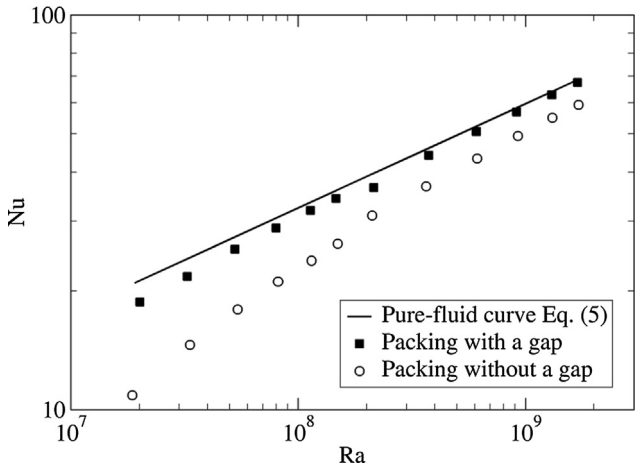

Fig. 5. Nu-Ra data for porous media consisting of 15.3 mm polypropylene spheres with and without a gap of $w/H = 0.10$ from the active walls. The solid line represents the pure-fluid reference curve, Eq. (5).

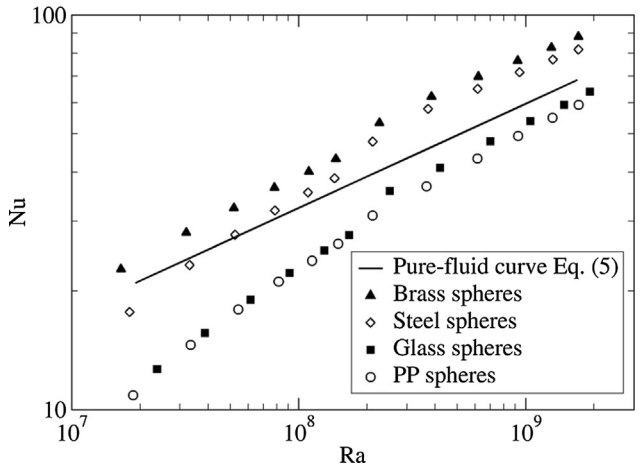

Fig. 6. Effect of sphere conductivity. Nu-Ra data for porous media consisting of 15.3 mm ($d/H = 0.20$) spheres in BCT packing with different conductivities compared to the pure-fluid reference curve.

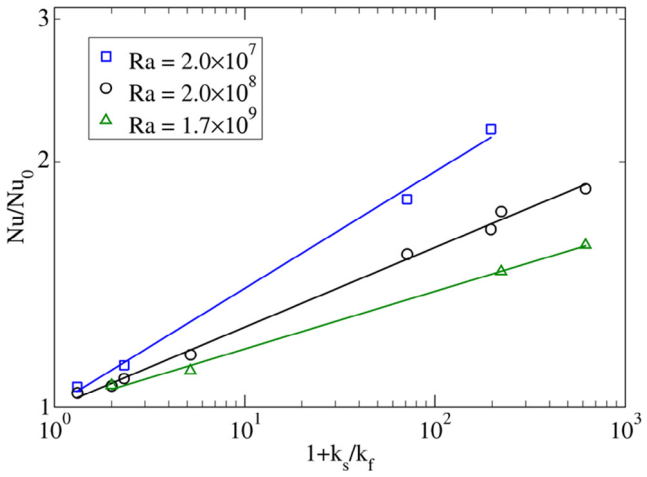

Fig. 7. Effect of the solid-to-fluid conductivity ratio on the Nusselt number at three different Rayleigh numbers Ra = 2.0×10^7, 2.0×10^8, and 1.7×10^9. The solid lines denote the fits to the data and represent $Nu = 10.6(1 + k_s/k_f)^{0.14}$, $Nu = 28.8(1 + k_s/k_f)^{0.10}$, $Nu = 55.6(1 + k_s/k_f)^{0.07}$, respectively.

of the slope m value in Eq. (6) with increasing Rayleigh number, being 0.14, 0.10, and 0.07 for the low, intermediate, and high Rayleigh numbers, respectively. This behavior indicates that at higher Rayleigh numbers conduction through the solid structure of a porous medium becomes less important compared to fluid convection.

3.1.5. Heat transfer scaling based on porous medium dimensionless numbers

The heat transfer data for eight different solid-fluid combinations reported in the previous section cover a wide range of porous medium Rayleigh numbers $10^2 < Ra_m < 10^5$ (see Eq. (3) for definition), and porous medium conductivity ratios $0.79 \leq k_{eff}/k_f \leq 17.3$ (see Section 2 for definition and Table 1). Fig. 8 shows $Nu_m (k_{eff}/k_f)^{0.49}$ versus Ra_m for all combinations of solids and fluids considered in this study. It is seen that for coarse-grained porous media consisting of $d/H = 0.20$ spheres, Nu_m is correlated to Ra_m and k_{eff}/k_f by the following relation

$$Nu_m = 1.349 Ra_m^{0.325} (k_{eff}/k_f)^{-0.49}. \quad (7)$$

The exponent of Ra_m is found to be 0.325 which is in good agreement with the values that have been reported in the literature for the non-Darcy flow regime [9,10,26,27]. Eq. (7) also presents the scaling of Nu_m with the porous medium conductivity ratio (k_{eff}/k_f). This correlation confirms that the porous medium Nusselt number Nu_m cannot be described as a function of Ra_m only, but in addition, there is a strong dependence on thermal conductivity that is captured well by the term $(k_{eff}/k_f)^{-0.49}$. The porous medium Nusselt number Nu_m represents the ratio of the total heat transfer over the conduction heat transfer through the combined stagnant fluid plus porous solid medium. At increased thermal conductivity of the porous medium, a larger fraction of the heat is transferred by conduction compared to convection, and Nu_m (but not Nu) decreases. Overall, the above correlation can be used to determine Nusselt numbers for side-heated natural convection in coarse porous media for a wide range of conductivity ratios k_{eff}/k_f and porous medium Rayleigh numbers, Ra_m.

Fig. 9 shows $Nu_m (k_{eff}/k_f)^{0.49}$ versus Ra_m for porous media consisting of glass spheres with three different sizes ($d/H = 0.20$, 0.14, and 0.065). The curves fitted to the data show that for Ra_m higher than approximately 10^3, Nu_m scales with Ra_m to the power 0.33 for $d/H = 0.20$ glass spheres, and to the power 0.36 for $d/H = 0.14$ glass spheres. For smaller $d/H = 0.065$ glass spheres, we observe a transition from a power 0.64 at Ra_m lower than approximately 10^3, to a smaller power of 0.42 at higher Ra_m. Such a decrease in the slope of the Nu_m-Ra_m relation with increasing d/H or Ra_m is due to the breakdown of the Darcian behavior and was also observed in other experimental studies which reported values for the Ra_m exponent from 0.61 to 0.64 [27,28] in the Darcy regime to 0.28–0.33 [9,10,27] when deviating from the Darcy regime at high Ra_m and for larger grains. Theoretical studies suggest a decrease in the slope of the Nu_m-Ra_m relation, with Nu_m proportional to $Ra_m^{1/2}$ in the Darcy limit [5] and to $Ra_m^{1/4}$ in the non-Darcy limit [29]. Our present study suggests that for large spheres ($d/H = 0.14$–0.20) and Ra_m larger than approximately 10^3 the flow is non-Darcian, whereas for smaller spheres ($d/H = 0.065$) a transition from Darcy to non-Darcy behavior occurs around $Ra_m = 10^3$.

3.2. Velocity and temperature distribution

PIV and LCT measurement techniques were used to provide insight into the pore-scale flow and heat transfer in differentially side heated coarse porous media. The resulting velocity and temperature fields are reported in this section.

3.2.1. Velocity fields

Fig. 10 shows the mean velocity fields in the pure-water cavity (left) and in the cavity filled with 15.3 mm ($d/H = 0.20$) hydrogel

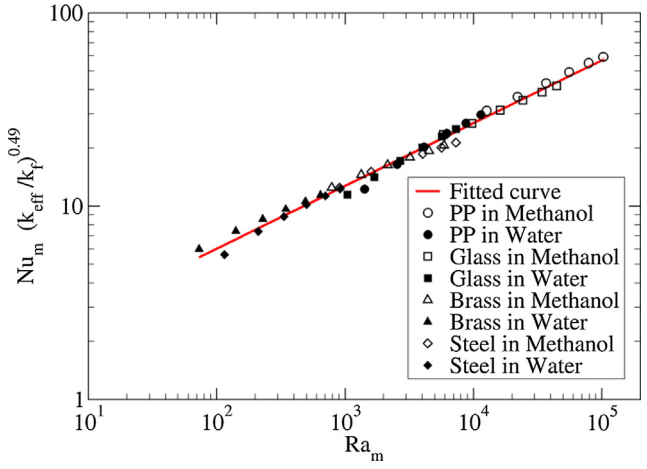

Fig. 8. Heat transfer data based on porous medium dimensionless numbers. $Nu_m (k_{eff}/k_f)^{0.49}$ versus Ra_m for eight different solid–fluid combinations for 15.3 mm ($d/H = 0.20$) spheres. The red line denotes the fit to the data.

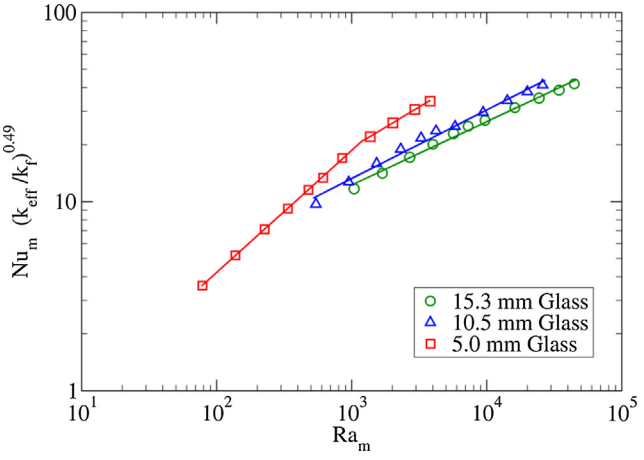

Fig. 9. Heat transfer data based on porous medium dimensionless numbers for three different glass sphere sizes ($d/H = 0.20$, 0.14, and 0.065). The solid lines denote power-law fits to the data.

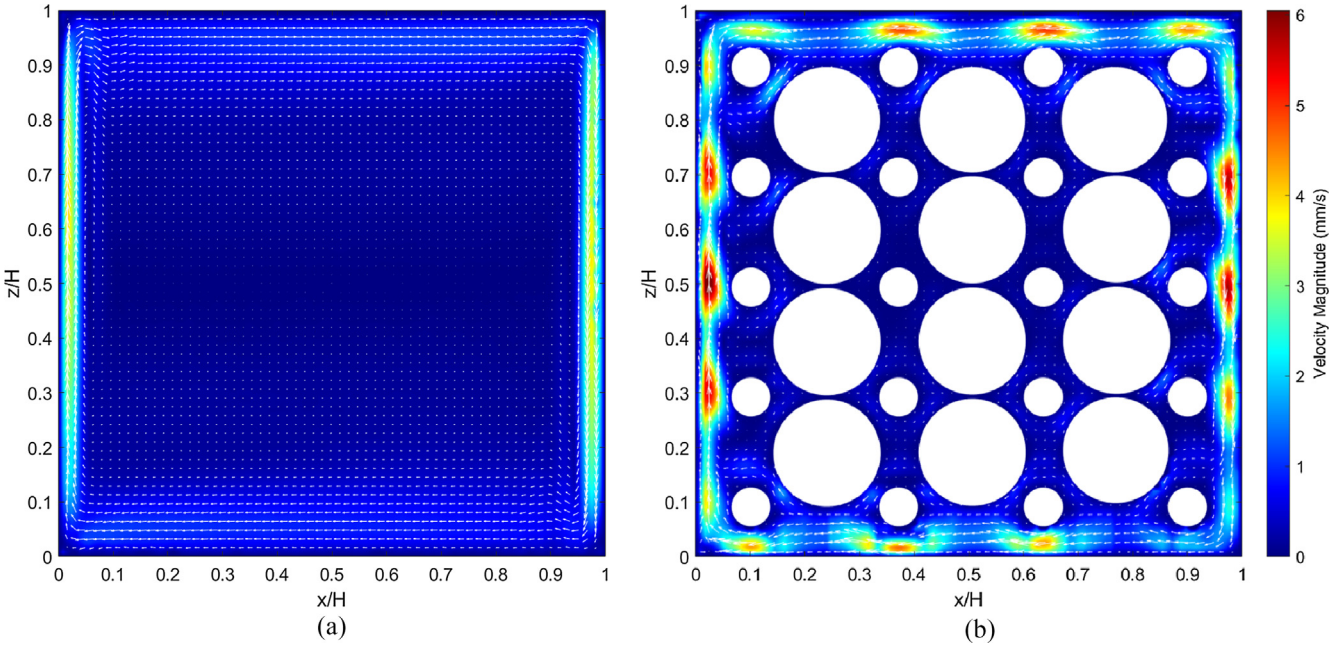

Fig. 10. Mean velocity field at Ra = 9.0×10^7 (a) in the pure-water cavity, and (b) in the cavity filled with 15.3 mm hydrogel spheres in BCT packing.

spheres in BCT packing (right) at Ra = 9.0×10^7. The mean velocity fields were obtained by averaging over 7200 image pairs that were taken at 1 Hz. The color map represents the distribution of velocity magnitude. The velocity field in the pure-water side-heated cavity is dominated by thin high-velocity boundary layers close to the thermally active hot and cold vertical walls. The flow along the horizontal walls occurs in much thicker layers with much lower velocities, while the flow in the core of the cavity is quiescent. These results are consistent with what has been reported in other studies on pure-fluid differentially heated natural convection at similar Rayleigh numbers [23,30,31].

Fig. 10 shows that in the presence of the coarse porous medium consisting of relatively large solid spheres, the development of a thin high-velocity layer along the vertical walls is substantially hindered. Instead, a wavy behavior with local maxima and minima in velocity is observed. This wavy behavior is also visible in Fig. 12, which presents the vertical velocity component (v_z) along a vertical line very close to the hot wall at $x/H = 0.03$. In Fig. 11 the velocity magnitude color map is shown on a logarithmic scale in order to be able to observe the flow distribution in the regions away from the walls. It shows that a portion of the fluid penetrates into the adjacent pores and is thus channeled away from the main stream along

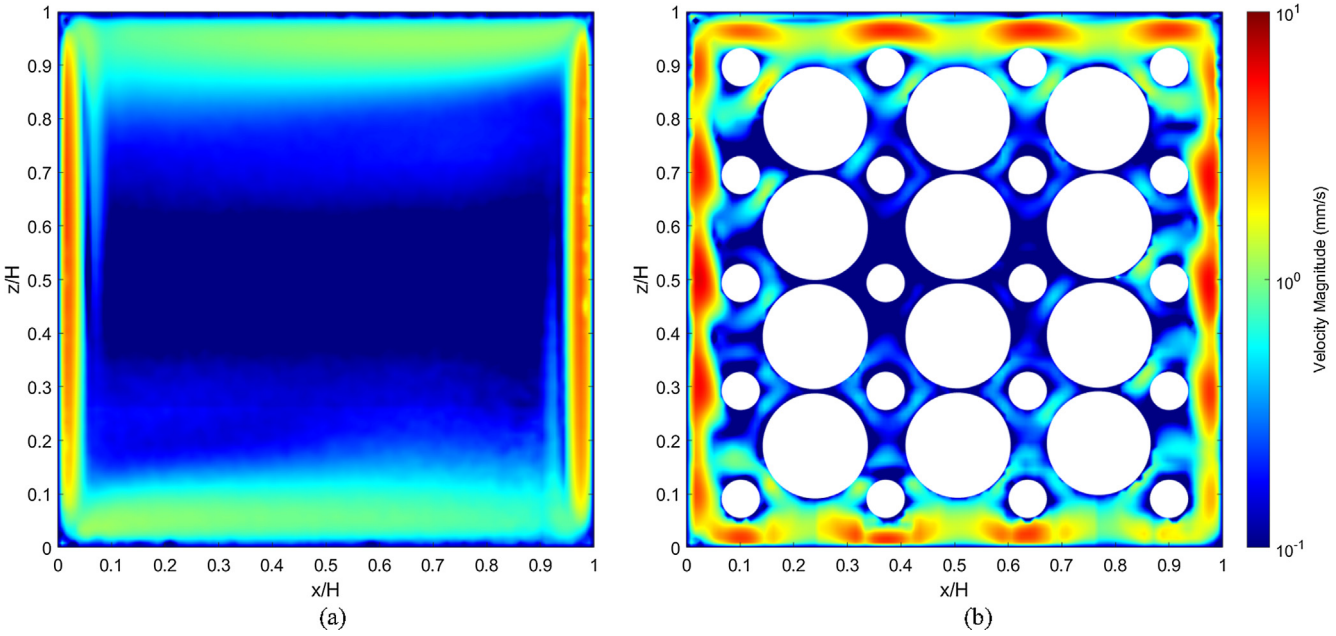

Fig. 11. Mean velocity magnitude shown on a logarithmic scale at Ra = 9.0×10^7 (a) in the pure-water cavity, and (b) in the cavity filled with 15.3 mm hydrogel spheres in BCT packing.

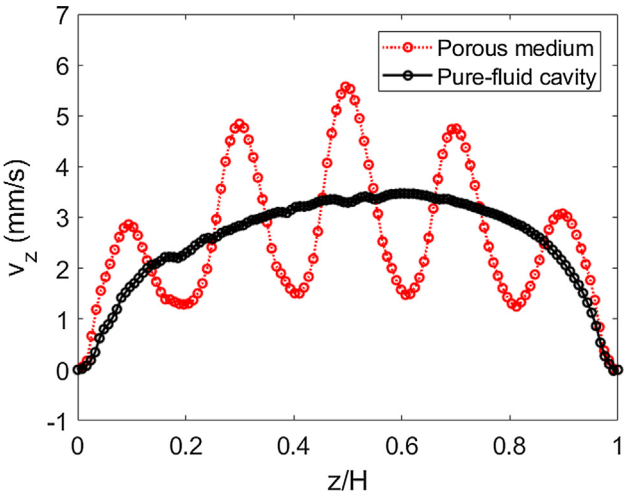

Fig. 12. Mean vertical velocity v_z along a vertical line close to the hot wall at $x/H = 0.03$ for the pure-water cavity (black markers), and for the cavity filled with hydrogel spheres (red markers) at Ra = 9.0×10^7.

the active hot/cold walls. Consequently, there is less interaction between the fluid and the hot/cold walls, which contributes to the heat transfer reduction with respect to the pure-fluid cavity, see red crosses in Fig. 2. This also explains the heat transfer results for the case with a gap between the active vertical walls and the porous medium presented in Section 3.1.3. When the gap is sufficiently large to allow for the formation of the thin high-velocity boundary layer, the heat transfer reduction will be small.

To make a quantitative comparison of the local velocity distributions for the two studied cases, Fig. 13 depicts profiles of the vertical velocity component (v_z) along three horizontal lines at $z/H = 0.5$, 0.6, and 0.7. The velocity profiles in Fig. 13 as well as in Fig. 12 show that the local velocity can be higher or lower depending on the vertical position.

Fig. 14 shows profiles of the horizontal velocity component (v_x) along three vertical lines at $x/H = 0.37$, 0.50, and 0.63 for the pure-water and hydrogel sphere filled cavity. The results in this figure and in Fig. 10 show that in the pure-water cavity the horizontal flow from one side of the cavity to the opposite side occurs over a relatively thick layer with relatively low velocities. In the cavity filled with spheres, the horizontal flow is more concentrated near the horizontal walls with significantly higher maximum velocities. (i.e. a factor of about 4.5 higher maximum horizontal velocity compared to the pure-water cavity). The slight heat transfer reduction observed in Fig. 5 (Section 3.1.3) for the case in which there is a gap between the vertical walls and the packing, relative to the pure-fluid cavity, could be due to the fact that the horizontal flow is hindered and confined to the region between the spheres and the horizontal walls. According to the heat transfer results, the hindering effect of the porous medium in the horizontal direction only accounts for 22% (at the lowest Ra) and 4.8% (at the highest Ra) of the total heat transfer reduction.

3.2.2. Temperature fields

Fig. 15 shows the mean temperature fields obtained from LCT measurements in the pure-water cavity (left) and in the cavity filled with 15.3 mm ($d/H = 0.20$) hydrogel spheres in BCT packing (right). In both cases, the temperatures of the cold and hot walls were 20.0 °C and 30.2 °C, respectively, leading to Ra = 9.0×10^7. The temperature field in the pure-water cavity shown in Fig. 15a illustrates the characteristic stratification in the core of the cavity and the thin thermal boundary layers along the vertical hot/cold walls. The stratified temperature distribution was also reported

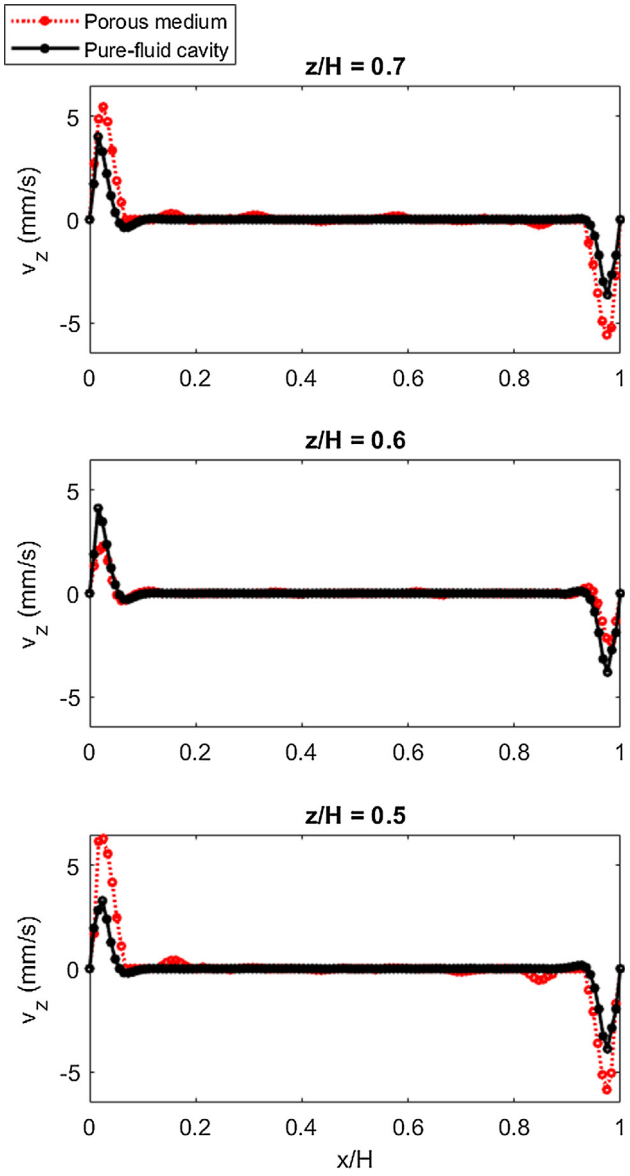

Fig. 13. Mean vertical velocity v_z along horizontal lines ($z/H = 0.50$, 0.60, and 0.70) for the pure-water cavity (black markers), and for the cavity filled with hydrogel spheres (red markers) at Ra = 9.0×10^7.

in previous studies on differentially heated natural convection in pure-fluid cavities at similar Rayleigh numbers [23,31]. The temperature field in the cavity filled with spheres shown in Fig. 15b is very different from that in the pure-water cavity. While in the pure-water cavity isotherms are horizontal, in the cavity filled with spheres, these are tilted with the temperature gradient roughly in the diagonal direction. The reason is that a portion of the high-velocity flow near the hot/cold vertical walls diverts away from the walls and penetrates into the pores and subsequently moves diagonally towards the opposite corner. This is consistent with the observations in the velocity fields in Fig. 11. The absence of temperature stratification also implies that the overall strength of convection decrease in the cavity filled with spheres, which leads to a reduced convective heat transfer as evidenced in the Nu-Ra results. Fig. 16 compares the fluid temperature profiles averaged over vertical lines spanning the entire height of the cavity (H) for the pure-water cavity and the cavity filled with spheres (excluding the locations occupied by the spheres), as a function of x/L. It can be seen that in the pure-water cavity, the temperature

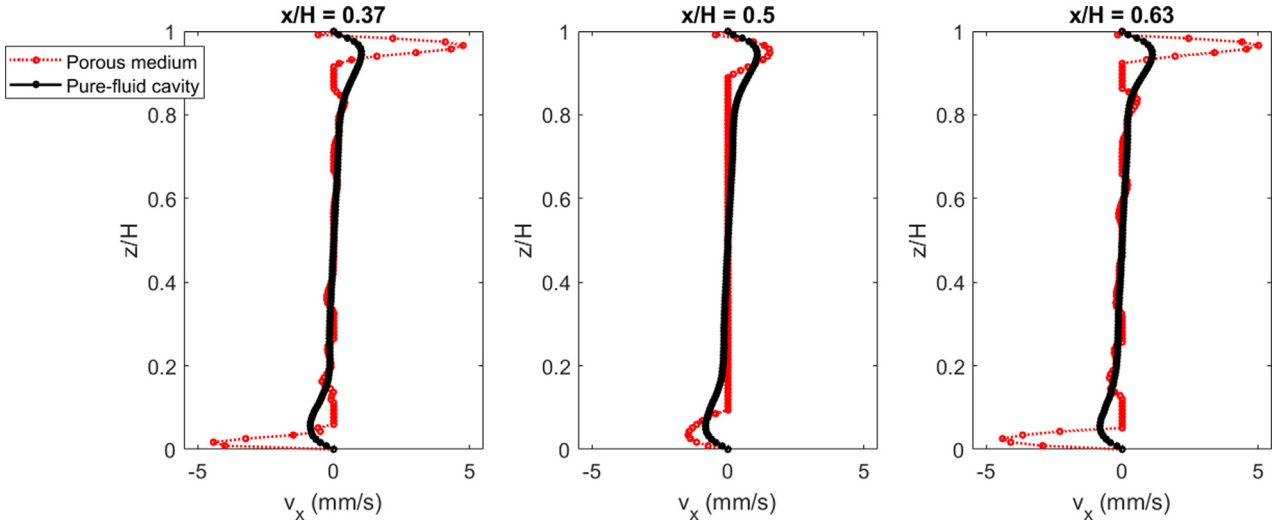

Fig. 14. Mean horizontal velocity v_x along three vertical lines (x/H = 0.37, 0.50, and 0.63) for the pure-water cavity (black markers), and for the cavity filled with hydrogel spheres (red markers) at Ra = 9.0×10^7.

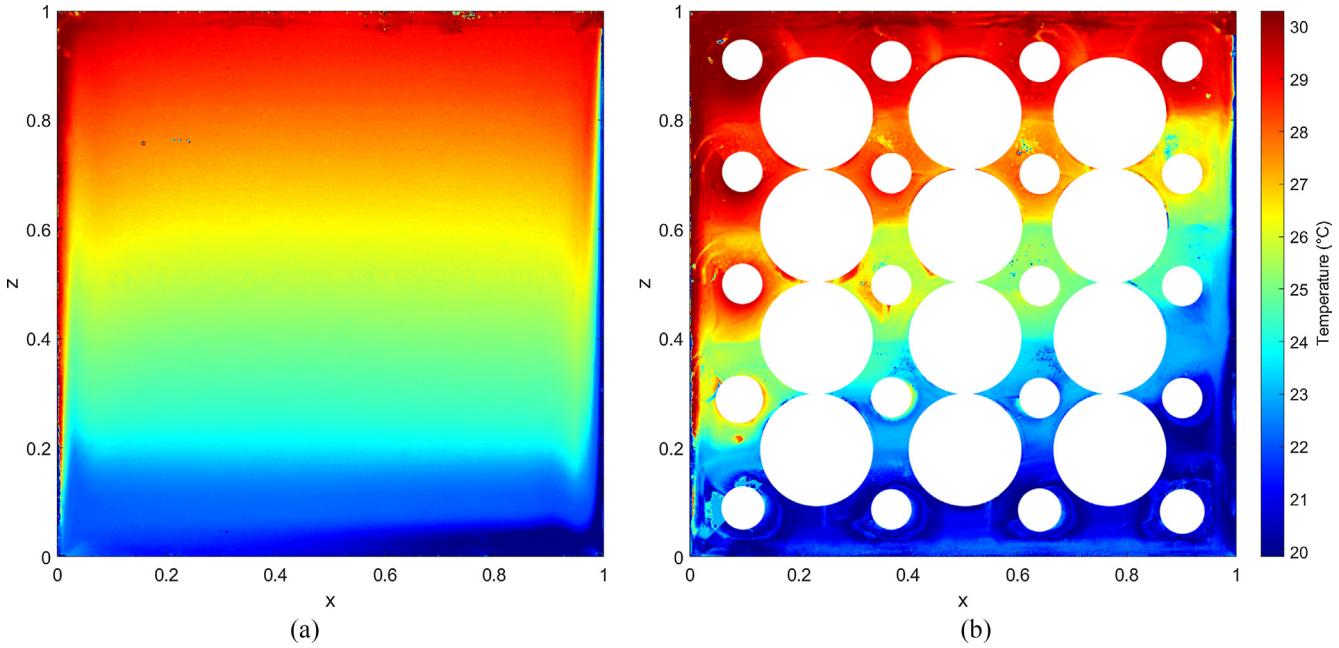

Fig. 15. Mean temperature fields (a) in the pure-water cavity, and (b) in the cavity filled with hydrogel spheres of 15.3 mm diameter in BCT packing. The temperatures of the cold and hot side walls were 20.0 °C and 30.2 °C, respectively, resulting in a Rayleigh number of Ra = 9.0×10^7.

profile is nearly horizontal in the core region of the cavity and significant temperature variations take place only in the thin thermal boundary layers close to the hot/cold walls. In the cavity filled with spheres, the vertically-averaged fluid temperature profile clearly reflects the presence of the spheres, and on average varies much more gradually from one vertical plate to the other. Fig. 17 compares the vertically-averaged fluid temperature profiles in a narrow region near the cold wall $0.965 \leq x/H \leq 1$. (The cold wall is chosen due to the higher color-temperature sensitivity of the liquid crystals in the colder part of the effective temperature range which leads to higher accuracy.) This figure shows that the gradient of the vertically-averaged temperature profile near the cold wall is smaller for the cavity filled with spheres compared to that for the pure-water cavity. The overall Nusselt number is defined as $Nu = q_{av} H/(k_f \Delta T)$ where q_{av} is the average heat flux (in W/m^2) at the cold wall. The heat flux at the cold wall is proportional to the slope of the vertically-averaged temperature profile (Fig. 17) at the wall at $x/H = 1$, i.e. $q_{av} = -k_f \, (dT_{av}/dx)|_{x=H}$. The reduced slope of the vertically-averaged temperature profile at the cold wall illustrates the reduced Nusselt number due to the presence of the porous medium. Fig. 17 shows that the slope of the vertically-averaged temperature profile at the cold wall for the cavity filled with spheres is approximately 30% smaller than that for the pure-water cavity which is consistent with the 30% reduction of heat transfer at the same Rayleigh number seen in Fig. 2 (red crosses). To study the temperature distributions at the cold wall in more detail, and to better understand the behavior of the temperature profiles at different heights, Fig. 18 shows temperature profiles along four horizontal lines at z/H = 0.2, 0.4, 0.6, and 0.8. It can be seen that in the upper part of the cold wall at

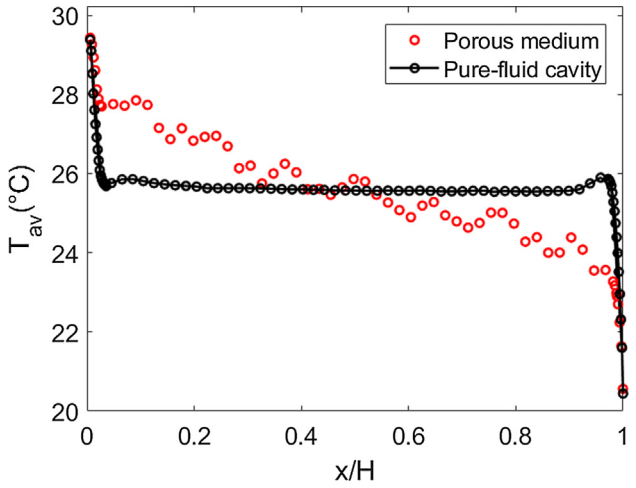

Fig. 16. Vertically-averaged fluid temperature profiles for the pure-water cavity (black markers), and for the cavity filled with hydrogel spheres (red markers) at Ra = 9.0×10^7.

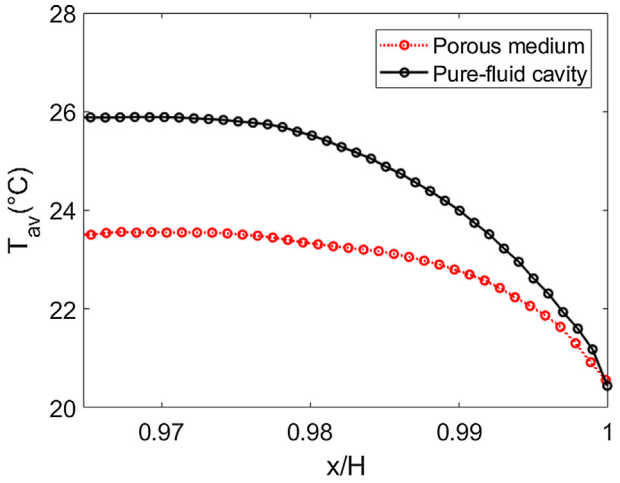

Fig. 17. Vertically-averaged fluid temperature profiles at the cold wall for the pure-water cavity (black markers), and for the cavity filled with hydrogel spheres (red markers) at Ra = 9.0×10^7.

$z/H = 0.8$ the temperature gradients near the cold wall are very high for both cases and even higher for the cavity filled with spheres. This leads to a high heat flux in the upper part of the cold wall for both cases. However, when moving towards the bottom of the cavity, the temperature gradient at the cold wall reduces more significantly for the cavity filled with spheres compared to the pure-water cavity. At $z/H = 0.2$, the temperature is almost uniform near the cold wall so that the heat flux is almost zero at the lower part of the cold wall in the cavity filled with spheres. On the other hand, for the pure-water cavity, the heat flux reduces to a lesser extent from top to the bottom and there is a considerable temperature gradient at $z/H = 0.2$. This implies that the local Nusselt number at the hot and cold walls is less uniform for the cavity filled with spheres, and that the reduction in overall Nusselt number for the cavity filled with spheres is mostly caused by the very low heat flux in the lower part of the cold wall (and the upper part of the hot wall).

4. Conclusions

Natural convection flow and heat transfer in a differentially side heated cubic cavity filled with coarse porous media consisting of relatively large spheres were studied experimentally. Nusselt numbers were measured for fluid Rayleigh numbers varying between 10^7 and 10^9, solid-to-fluid conductivity ratios ranging from 0.32 to 618, three different sphere sizes ($d/H = 0.065$, 0.14, 0.20), and three different packing types (body-centered tetragonal, simple cubic, and random). A partially-filled cavity with a gap between the porous medium and the hot/cold walls was also considered.

It was found that the Nusselt number is reduced in the cavity filled with spheres compared to the pure-fluid cavity, unless the solid spheres are highly conductive. The Nusselt number reduction is higher for smaller spheres and is not very sensitive to the packing type, especially at high Rayleigh numbers. For the porous medium with a gap between the hot/cold walls and the spheres, the heat transfer reduction is significantly smaller and the Nusselt numbers reach those for the pure-fluid cavity at the highest Rayleigh numbers ($Ra > 10^9$). The following Nusselt number correlation was derived for coarse porous media with $d/H = 0.2$

$$Nu_m = 1.349 Ra_m^{0.325} (k_{eff}/k_f)^{-0.49}$$

for porous medium Rayleigh numbers $10^2 < Ra_m < 10^5$ and porous medium conductivity ratios $0.79 \leq k_{eff}/k_f \leq 17.3$. This expression takes into account the strong dependence of the porous medium Nusselt number on the porous medium conductivity ratio, and its scaling with the porous medium Rayleigh number is consistent with the power-law scaling reported in the literature for the non-Darcy regime.

Measured velocity and temperature fields show that the layers of spheres close to the vertical hot/cold walls hinder the formation

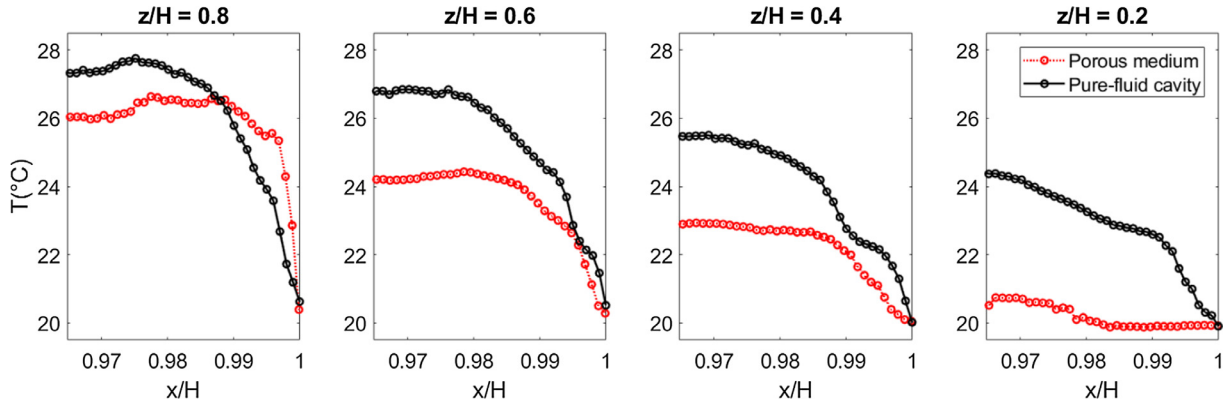

Fig. 18. Temperature profiles along four horizontal lines ($z/H = 0.2$, 0.4, 0.6, and 0.8) for the pure-water cavity (black markers), and for the cavity filled with hydrogel spheres (red markers) at Ra = 9.0×10^7.

of high-velocity boundary layers and divert a portion of the fluid away from these walls towards the inner pores. This phenomenon reduces the temperature stratification in the core of the cavity and leads to a reduced mean temperature gradient at the walls, which explains the heat transfer reduction in porous media.

It is also concluded that, although the overall Nusselt number is lower for the cavity filled with a coarse-grained porous medium, the local Nusselt number at the cold/hot walls can be significantly higher than in the corresponding pure-fluid cavity. The presence of a coarse-grained porous medium thus causes strong non-uniformities in the local wall heat transfer, leading to so-called hot-spots which may have severe consequences in practical applications such as lowering the lifespan of blast furnace refractory walls.

Declaration of Competing Interest

The authors declared that there is no conflict of interest.

Acknowledgments

This research was carried out under project number S41.5.14526b in the framework of the Partnership Program of the Material innovation institute M2i (www.m2i.nl) and the Technology Foundation TTW (www.stw.nl), which is part of the Netherlands Organization for Scientific Research (www.nwo.nl). We also thank the industrial partner of the project Tata Steel in Europe. We thank the research technician Bart Hoek for his contribution to the design and preparation of the experimental setup.

References

[1] V. Panjkovic, J.S. Truelove, P. Zulli, Numerical modelling of iron flow and heat transfer in blast furnace hearth, Ironmak. Steelmak. 29 (2002) 390–400, https://doi.org/10.1179/030192302225005187.
[2] O. Laguerre, S. Ben Amara, J. Moureh, D. Flick, Numerical simulation of air flow and heat transfer in domestic refrigerators, J. Food Eng. 81 (2007) 144–156, https://doi.org/10.1016/j.jfoodeng.2006.10.029.
[3] J.T. Hu, X.H. Ren, D. Liu, F.Y. Zhao, H.Q. Wang, Conjugate natural convection inside a vertical enclosure with solid obstacles of unique volume and multiple morphologies, Int. J. Heat Mass Transf. 95 (2016) 1096–1114, https://doi.org/10.1016/j.ijheatmasstransfer.2015.12.070.
[4] K. Horikiri, Y. Yao, J. Yao, Numerical optimisation of thermal comfort improvement for indoor environment with occupants and furniture, Energy Build. 88 (2015) 303–315, https://doi.org/10.1016/j.enbuild.2014.12.015.
[5] J.E. Weber, The boundary-layer regime for convection in a vertical porous layer, Int. J. Heat Mass Transf. 18 (1975) 569–573, https://doi.org/10.1016/0017-9310(75)90298-7.
[6] G. Lauriat, V. Prasad, Non-Darcian effects on natural convection in a vertical porous enclosure, Int. J. Heat Mass Transf. 47 (1989) 2135–2148.
[7] C. Beckermann, R. Viskanta, S. Ramadhyani, A numerical study of non-darcian natural convection in a vertical enclosure filled with a porous medium, Numer. Heat Transf. 10 (1986) 557–570, https://doi.org/10.1080/10407788608913535.
[8] G. Lauriat, V. Prasad, Natural convection in a vertical porous cavity: a numerical study for brinkman-extended darcy formulation, J. Heat Transf. 109 (1987) 688, https://doi.org/10.1115/1.3248143.
[9] N. Seki, S. Fukusako, H. Inaba, Heat transfer in a confined rectangular cavity packed with porous media, Int. J. Heat Mass Transf. 21 (1978) 985–989, https://doi.org/10.1016/0017-9310(78)90190-4.
[10] K.J. Schneider, Investigation of the influence of free thermal convection on heat transfer through granular material, in: Proc. 11th Int. Congr. Refrig., 1963, p. 4.
[11] A.A. Merrikh, J.L. Lage, Natural convection in an enclosure with disconnected and conducting solid blocks, Int. J. Heat Mass Transf. 48 (2005) 1361–1372, https://doi.org/10.1016/j.ijheatmasstransfer.2004.09.043.
[12] E.J. Braga, M.J.S. De Lemos, Heat transfer in enclosures having a fixed amount of solid material simulated with heterogeneous and homogeneous models, Int. J. Heat Mass Transf. 48 (2005) 4748–4765, https://doi.org/10.1016/j.ijheatmasstransfer.2005.05.016.
[13] D. Iyi, R. Hasan, R. Penlington, Experimental and numerical study of Buoyancy-driven low turbulence flow in rectangular enclosure partially filled with isolated solid blockages, Int. J. Heat Mass Transf. 127 (2018) 534–545, https://doi.org/10.1016/j.ijheatmasstransfer.2018.07.031.
[14] A. Raji, M. Hasnaoui, M. Naïmi, K. Slimani, M.T. Ouazzani, Effect of the subdivision of an obstacle on the natural convection heat transfer in a square cavity, Comput. Fluids 68 (2012) 1–15, https://doi.org/10.1016/j.compfluid.2012.07.014.
[15] M.A. Delele, E. Tijskens, Y.T. Atalay, Q.T. Ho, H. Ramon, B.M. Nicolaï, P. Verboven, Combined discrete element and CFD modelling of airflow through random stacking of horticultural products in vented boxes, J. Food Eng. 89 (2008) 33–41, https://doi.org/10.1016/j.jfoodeng.2008.03.026.
[16] F. Bambauer, S. Wirtz, V. Scherer, H. Bartusch, Transient DEM-CFD simulation of solid and fluid flow in a three dimensional blast furnace model, Powder Technol. 334 (2018) 53–64, https://doi.org/10.1016/j.powtec.2018.04.062.
[17] O. Laguerre, S. Ben Amara, G. Alvarez, D. Flick, Transient heat transfer by free convection in a packed bed of spheres: comparison between two modelling approaches and experimental results, Appl. Therm. Eng. 28 (2008) 14–24, https://doi.org/10.1016/j.applthermaleng.2007.03.014.
[18] M.D. Shattuck, R.P. Behringer, G.A. Johnson, J.G. Georgiadis, Convection and flow in porous media. Part 1. Visualization by magnetic resonance imaging, J. Fluid Mech. 332 (1997) 215–245, https://doi.org/10.1017/S0022112096003990.
[19] O. Laguerre, S. Benamara, D. Remy, D. Flick, Experimental and numerical study of heat and moisture transfers by natural convection in a cavity filled with solid obstacles, Int. J. Heat Mass Transf. 52 (2009) 5691–5700, https://doi.org/10.1016/j.ijheatmasstransfer.2009.07.028.
[20] I. Ataei-Dadavi, M. Chakkingal, S. Kenjeres, C.R. Kleijn, M.J. Tummers, Flow and heat transfer measurements in natural convection in coarse-grained porous media, Int. J. Heat Mass Transf. 130 (2019) 575–584, https://doi.org/10.1016/j.ijheatmasstransfer.2018.10.118.
[21] M. Chakkingal, S. Kenjereš, I. Ataei-Dadavi, M.J. Tummers, C.R. Kleijn, Numerical analysis of natural convection with conjugate heat transfer in coarse-grained porous media, Int. J. Heat Fluid Flow 77 (2019) 48–60, https://doi.org/10.1016/j.ijheatfluidflow.2019.03.008.
[22] S. Ergun, Fluid flow through packed columns, Chem. Eng. Prog. 48 (1952) 89–94.
[23] P. Wang, Y. Zhang, Z. Guo, Numerical study of three-dimensional natural convection in a cubical cavity at high Rayleigh numbers, Int. J. Heat Mass Transf. 113 (2017) 217–228, https://doi.org/10.1016/j.ijheatmasstransfer.2017.05.057.
[24] E. Tric, G. Labrosse, M. Betrouni, A first incursion into the 3D structure of natural convection of air in a differentially heated cubic cavity, from accurate numerical solutions, Int. J. Heat Mass Transf. 43 (2000) 4043–4056, https://doi.org/10.1016/S0017-9310(00)00037-5.
[25] J. Patterson, J. Imberger, Unsteady natural convection in a rectangular cavity, J. Fluid Mech. 100 (1980) 65, https://doi.org/10.1017/s0022112080001012.
[26] V. Prasad, A. Tuntomo, Inertia effects on natural convection in a vertical porous cavity, Numer. Heat Transf. 11 (1987) 295–320, https://doi.org/10.1080/10407788708913556.
[27] V. Prasad, F.A. Kulacki, M. Keyhani, Natural convection in porous media, J. Fluid Mech. 150 (1985) 89, https://doi.org/10.1017/s0022112085000040.
[28] R.M. Fand, T.E. Steinberger, P. Cheng, Natural convection heat transfer from a horizontal cylinder embedded in a porous medium, Int. J. Heat Mass Transf. 29 (1986) 119–133, https://doi.org/10.1016/0017-9310(86)90040-2.
[29] D. Poulikakos, A. Bejan, The departure from Darcy flow in natural convection in a vertical porous layer, Phys. Fluids 28 (1985) 3477, https://doi.org/10.1063/1.865301.
[30] M.R. Ravi, R.A.W.M. Henkes, C.J. Hoogendoorn, On the high-Rayleigh-number structure of steady laminar natural-convection flow in a square enclosure, J. Fluid Mech. 262 (1994) 325, https://doi.org/10.1017/s0022112094000522.
[31] Y.S. Tian, T.G. Karayiannis, Low turbulence natural convection in an air filled square cavity: Part I: the thermal and fluid flow fields, Int. J. Heat Mass Transf. 43 (2000) 849–866, https://doi.org/10.1016/S0017-9310(99)00199-4.